Rational design of a metal–organic framework host for sulfur storage in fast, long-cycle Li–S batteries

ARTICLE *in* ENERGY & ENVIRONMENTAL SCIENCE · JULY 2014

Impact Factor: 20.52 · DOI: 10.1039/C4EE01382D

9 AUTHORS, INCLUDING:

Junwen Zhou
Peking University
11 PUBLICATIONS **65** CITATIONS
SEE PROFILE

Jie Zheng
Peking University
81 PUBLICATIONS **1,277** CITATIONS
SEE PROFILE

Bo Wang
Beijing Institute of Technology
51 PUBLICATIONS **3,188** CITATIONS
SEE PROFILE

Energy & Environmental Science

PAPER

View Article Online
View Journal | View Issue

Cite this: *Energy Environ. Sci.*, 2014, **7**, 2715

Rational design of a metal–organic framework host for sulfur storage in fast, long-cycle Li–S batteries†

Junwen Zhou,[a] Rui Li,[b] Xinxin Fan,[a] Yifa Chen,[b] Ruodan Han,[b] Wei Li,[a] Jie Zheng,[a] Bo Wang*[b] and Xingguo Li*[a]

Received 4th May 2014
Accepted 3rd June 2014

DOI: 10.1039/c4ee01382d

www.rsc.org/ees

Unlike an intercalation cathode, which has an intrinsic host structure made of redox metal sites allowing the transport of Li^+/e^-, sulfur as a conversion cathode requires an additional host to store and immobilize the mobile redox centers, polysulfides. Metal–organic frameworks (MOFs) as a class of highly porous and well-defined crystalline materials are a promising platform to search for an effective host through rational design. With the appropriate selection of an electrolyte and a cutoff voltage range, sulfur stored in an appropriate MOF host can take advantage of both intercalation (fast and stable) and conversion (high energy density) cathodes. Herein, we describe a fast cathode with long cycle life based on sulfur and ZIF-8 nanocrystals. With 30 wt% sulfur loading in the electrode, it achieves remarkable discharge capacities of 1055 mA h g^{-1} (based on sulfur) at 0.1 C and 710 mA h g^{-1} at 1 C. The decay over 300 cycles at 0.5 C is 0.08% per cycle, prominent in long-cycle Li–S batteries. By comparing with another three distinct MOFs, MIL-53 (Al), NH_2-MIL-53 (Al) and HKUST-1, as well as two sets of ZIF-8 with particle sizes in the micrometer range, it reveals that (i) the small particle size of the MOF host is appreciable to achieve a high capacity and (ii) small apertures, associated with functionalities in the open framework that have affinity with the polysulfide anions, can help achieve a stable cycling. We believe that the findings are general and applicable for the rational design of new hosts for sulfur in other porous material families to produce more effective and stable Li–S batteries.

Broader context

Sulfur is one of the most promising cathode materials for next generation high-energy-density battery systems. It provides a high theoretical capacity of 1675 mA h g^{-1} with specific energy of 2500 W h kg^{-1}, and is abundant and environmentally benign. However, the dissolution of the intermediate polysulfides during operation results in dramatic capacity fading and hinders the practical application of Li–S batteries. Therefore storage and immobilization of dissolved polysulfides is of central importance in designing a stable sulfur cathode. Metal–organic frameworks (MOFs) as a huge class of highly porous and well-defined crystalline materials give great opportunity to search for an effective host rationally and systematically. In this work we demonstrate the nanosized MOF material (ZIF-8) as an excellent host material to produce a fast sulfur cathode with long cycle life. Our findings may shed light on the selection of a suitable MOF host to get high capacity retention and show the importance of controlling the particle size of MOFs to achieve high sulfur utilization and rate capability.

Introduction

Having received great success in the past two decades in powering portable wireless devices such as mobile phones, laptops and digital cameras,[1,2] cathode materials of the first generation rechargeable lithium-ion batteries (LIBs) are well-established in intercalation chemistry. Such a cathode (*e.g.* $LiCoO_2$) consists of a host framework (layered host CoO_2 for $LiCoO_2$) into/from which the mobile cation (Li^+) is inserted/extracted reversibly.[3] Electron transfer occurs with the redox-active transition metal (Co^{IV}/Co^{III} for $LiCoO_2$) of the host, which is inevitably limited in capacity to one or at most two Li per host (only 0.5 for $LiCoO_2$).[4] For the growing demand in stored energy density for powering an electric vehicle (EV), attention has turned towards the use of inexpensive multielectron redox centers based on conversion chemistry, where discharge/charge of the electrode is coupled with cleavage/formation of covalent bonds.[3,5] Sulfur (S_8) is one of the most promising candidates. With two Li per S atom, it provides a high theoretical capacity of 1675 mA h g^{-1} and specific energy of 2500 W h kg^{-1}, at least 3–5 times that of intercalation cathodes.[5,6] Besides, it is abundant (with extremely low cost) and environmentally benign, both important for a new

[a]*Beijing National Laboratory for Molecular Sciences (BNLMS), The State Key Laboratory of Rare Earth Materials Chemistry and Applications, College of Chemistry and Molecular Engineering, Peking University, 5 Yiheyuan Road, Beijing, 100871, P.R. China. E-mail: xgli@pku.edu.cn*

[b]*Key Laboratory of Cluster Science, Ministry of Education of China, School of Chemistry, Beijing Institute of Technology, 5 South Zhongguancun Street, Beijing, 100081, P.R. China. E-mail: bowang@bit.edu.cn*

† Electronic supplementary information (ESI) available: Full synthetic procedures and characterization of other MOF and S/MOF samples. See DOI: 10.1039/c4ee01382d

energy economy.[6] However, due to the intrinsic nature of the overall redox couple, described by the reaction $S_8 + 16Li^+ + 16e^- \leftrightarrow 8Li_2S$, tremendous difficulties are involved in the design of such a conversion cathode with high specific capacity and long cycle life.[7] The first one is related to the utilization of active materials. Because sulfur and its reduction products (Li_2S_2 and Li_2S) are both electronically and ionically insulating, it is strictly required that they are always in good contact with the conductive matrix. This is particularly difficult to realize because polysulfides, the intermediate reaction species, are highly soluble in the electrolyte, which makes it easy for them to either react with the Li anode creating an internal shuttle phenomenon, or randomly precipitate on the cathode surface as insoluble agglomerates causing active mass loss. As a result, sulfur cathodes are often plagued with rapid capacity fading.

Unlike an intercalation cathode, which has an inherent host structure made of redox metal sites allowing the transport of Li^+/e^- with minor perturbation to the framework, sulfur as a conversion cathode requires an additional host to store and immobilize the mobile redox centers, namely, polysulfides.[8] Carbonaceous materials, such as porous carbon,[9,10] carbon nanofibers,[11,12] carbon nanotubes,[13,14] carbon spheres,[15,16] and various types of graphene,[17–19] have been extensively investigated as effective hosts in sulfur cathodes, for their high electronic conductivity and physical adsorption/absorption on polysulfides. Similar roles can be played by conducting polymers to get enhanced cycling stability.[20,21] Surface coating, with either polymer[22] or metal oxide,[23,24] is another strategy to provide a host. The coating layer serves as a physical barrier to prevent the polysulfides from leaving the cathode, yet in some cases at the expense of retarding the transport of Li^+/e^-.[23] The use of an adsorbing additive to reversibly capture and release polysulfides during operation is a design of an auxiliary host.[25,26] One notable example for this strategy is SBA-15,[25] termed as a "polysulfide reservoir" by the authors, which stabilizes the polysulfide anions through weak binding on the positively charged silica surface. A generalized host, with modifications of the cell configuration, is given by inserting a carbon paper between the cathode and the separator, which traps the polysulfides within the cathode region.[27,28] To sum up, a host material for sulfur storage must have a "smart" pore structure and a "suitable" chemical environment for an "appropriate" interaction with the polysulfide anions. Though the abovementioned materials have satisfied these requirements to a large extent, rational and systematic design and adjustment of the size, shape, functionality of the pores and thus interaction with the polysulfides in these materials is hard to carry out due to their synthetic methodologies.

Encouragingly, coworkers with Tarascon and Férey pioneered the use of metal–organic frameworks (MOFs) as host materials for sulfur storage, taking advantage of the weak binding between the polysulfides and the oxygenated framework.[29] By using a mesoporous MOF, MIL-100 (Cr), the authors showed a remarkable increase in capacity retention of the cell. After that, various groups have demonstrated that other MOFs can be adopted.[30–32] Since MOFs are a class of porous materials assembled by connecting metal ions and organic linkers with tremendous extensiveness in variety and multiplicity,[33–35] there is great opportunity to rationally design and systematically adjust for an effective MOF host to store sulfur and fully confine the mobile redox centers, supported by the state-of-the-art science and technology in the reticular chemistry.[35] Logical examinations of structure–property trends to suggest promising candidates are therefore desirable.

Yet to design an efficient MOF host for sulfur storage, factors beyond MOF structures also need considerations, as depicted in Fig. 1. Above all is the particle size of the host. Lessons from the intercalation cathode design tell us that the rate of Li^+/e^- transport can be significantly increased by reducing the dimensions of the material, because the characteristic time constant t for diffusion is proportional to the square of the diffusion length L ($t \approx L^2/D$), where D is the ion diffusivity;[2,4] thus small dimensions for the host are desired. Secondly, the Li^+/e^- transport is coupled with the reactions in the redox cascade; their kinetics: all-liquid ($Li_2S_8 \leftrightarrow Li_2S_6 \leftrightarrow Li_2S_4$) > liquid–solid ($S_8 \leftrightarrow Li_2S_8$, $Li_2S_4 \leftrightarrow Li_2S_2$) $\gg$ all-solid ($Li_2S_2 \leftrightarrow Li_2S$).[5,8] The kinetics, while influenced by the pore structure and chemical environment of the host, is also determined by the selection of the electrolyte[10,36] and the cutoff voltage range.[37] The existence of soluble polysulfides in the system is valuable for maintaining a fast kinetics, owing to the molecular nature of the species involved so that they can rapidly exchange Li^+/e^- with each other.[5,38] Comprehensive optimization of these factors can give birth to a fast and stable sulfur cathode, in which the mobile dielectron redox centers are well-confined in a well-defined host framework for the reversible insertion/extraction of Li^+/e^-. MOF here builds the bridge between intercalation and conversion cathodes.

Former MOF hosts[29–31] fall short in (i) fast initial decay during early cycling (30–70%), (ii) low working current density (most at 0.1 C), and (iii) low sulfur loading (<20 wt% in electrode). Herein, we demonstrate a fast sulfur cathode with long cycle life by using ZIF-8 nanocrystals as the host. With 30 wt% sulfur loading in the electrode, prominent discharge capacities of 1055 mA h g^{-1} (based on sulfur) at 0.1 C and 710 mA h g^{-1} at 1 C are achieved in an electrolyte with low viscosity and high polysulfide solubility. Most impressively, the capacity decay over 300 cycles at 0.5 C is as small as 0.08% per cycle, among the

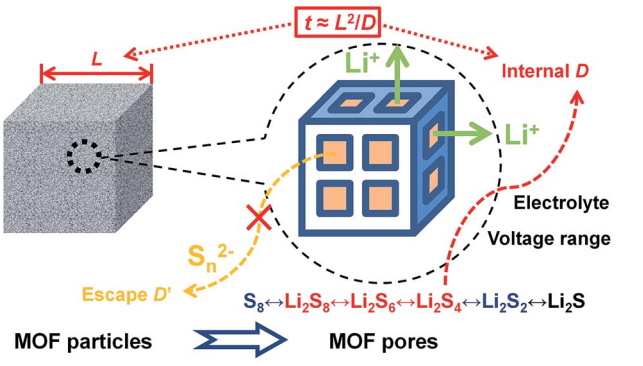

Fig. 1 Factors for consideration in the rational design of a fast and stable cathode made from MOF and sulfur.

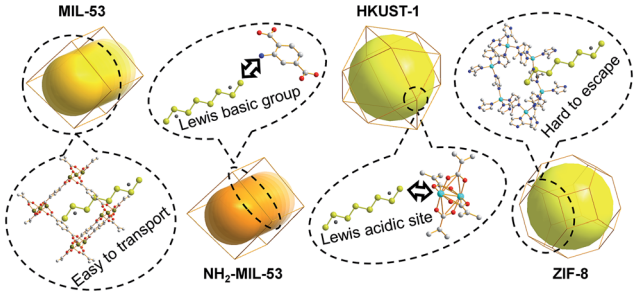

Fig. 2 Schematic of the MOFs chosen in this study and their unique characteristics.

excellent retentions in long-cycle Li–S batteries. It is also worth noting that by testing within 1.8–2.8 V, rapid initial decays are generally avoided.

To broaden our knowledge of how the structures of the MOF hosts are linked with their properties in the Li–S system, data are presented with another three distinct MOFs, MIL-53 (Al), NH_2-MIL-53 (Al), and HKUST-1. These MOFs represent a cross-section of unique characteristics such as the breathing network with 1D channels (MIL-53 (ref. 39) and NH_2-MIL-53 (ref. 40)), amine functionality (NH_2-MIL-53), unsaturated metal sites (HKUST-1 (ref. 41)) and cage-type pores with small apertures (ZIF-8 (ref. 42)), which are illustrated in Fig. 2. In particular, they all have reasonable thermal[39–42] and chemical stability toward sulfur and other chemicals involved in the synthetic procedures and electrochemical tests. It is also noteworthy that these MOFs are simple, scalable, and cost-effective: all are advantageous for practical use. To clarify the contribution of the MOF particle size to the electrochemical performance, two sets of homogeneous microsized ZIF-8 particles with different average sizes are used to compare with their nanosized counterpart.

Experimental section

Synthesis

MIL-53 (Al), NH_2-MIL-53 (Al), HKUST-1 as well as two sets of microsized ZIF-8 (denoted as ZIF-8-M and ZIF-8-L) were synthesized through solution methods.[43–45] Nanocrystals of ZIF-8 were yielded *via* a simple mechanochemical synthetic protocol.[46] In preparing a sulfur–MOF composite (S/MOF), sulfur was first ground with degassed MOF powders at a predetermined weight ratio (1 : 1), followed by a conventional melt diffusion process[9,29] under modified temperatures (for details see ESI†). All the degassed MOFs and S/MOF samples were kept in an argon-filled glove box prior to use.

Characterization

The structure and morphology of the samples were characterized by powder X-ray diffraction (PXRD, Rigaku D/max 2000 diffractometer, Cu Kα) and scanning electron microscopy (SEM, Hitachi S4800). Nitrogen adsorption–desorption isotherms were measured on a COULTER SA 3100 apparatus at 77 K. Before the measurement, MOF samples were degassed with the reported procedures;[42–44] S/MOF samples were measured immediately after leaving the glove box. Thermal gravimetric analysis (TGA) was carried out on a Q600 SDT thermoanalyzer (Thermal Analysis Corporation, USA) in N_2 with a heating rate of 10 °C min^{-1}: all samples were tested immediately after leaving the glove box.

Electrochemistry

To prepare the cathodes, 60 wt% S/MOF composite, 30 wt% conductive carbon black (CB) and 10 wt% poly(vinylidene fluoride) (PVDF) binder were mixed in *N*-methyl-2-pyrrolidinone (NMP) to form a slurry. The slurry was then coated on aluminium current collectors and dried at 60 °C over 24 h. Coin cells of 2032-type with a metallic Li anode were assembled. 0.6 M bis-(trifluoromethanesulfonyl)imide lithium (LiTFSI) in a mixed solvent of 1,2-dimethoxyethane (DME) and 1,3-dioxolane (DOL) (v/v 1 : 1) was used as the electrolyte with 0.1 M $LiNO_3$ as an additive to passivate the surface of the Li anode.[47] This electrolyte was chosen for its low viscosity and high polysulfide solubility.[48] The total amount of electrolyte added to each cell was 60 μL. The batteries were cycled galvanostatically with a LAND CT2001A instrument (Wuhan, China). Electrochemical impedance spectroscopy (EIS) measurements were performed on an electrochemical workstation (CH I660D, Shanghai Chenhua) within the frequency range of 100 kHz to 0.1 Hz with an AC voltage amplitude of 5 mV. The batteries were first discharged to 1.8 V then charged to 2.8 V at 0.1 C for activation. After that, EIS measurements were performed at 0%, ~20%, ~80% and 100% depth of discharge and then ~50%, ~80% and 100% depth of charge, subsequently, during the second cycle at 0.1 C. All the tests were carried out at room temperature.

Results and discussion

By virtue of the mechanochemical synthesis, ZIF-8 with uniform particle size (100–200 nm) and morphology were obtained (Fig. 3a), valuable for improving electrode homogeneity and integrity.[49,50] Scanning electron microscopy (SEM) studies suggested that the size and morphology of S/ZIF-8 (Fig. 3b) remain almost the same as ZIF-8 alone (Fig. 3a); no large sulfur agglomerates were found. However, closer observation reveals that some sulfur still exists in a highly dispersed state on the external surface, which is commonly unavoidable in one-step heating treatment.[16,17] Elemental mapping of sulfur in SEM also confirmed its uniform distribution (Fig. 3c). The impregnation of sulfur was next studied by powder X-ray diffraction (PXRD). As shown in Fig. 3d, the structure of ZIF-8 is well-maintained during the whole process; on the other hand, characteristic peaks for bulk crystalline sulfur become almost undetectable after the heating step, indicating the success of sulfur infiltration.[29] The sulfur infiltration was further investigated by nitrogen adsorption measurements[9] (Fig. 3e): S/ZIF-8 shows significant loss in porosity compared with pristine ZIF-8. The sulfur content, both calculated by the mass changes before and after the heating treatment[15] and measured by thermal gravimetric analysis (TGA, Fig. 3f), agrees well with the predetermined one (~50 wt% of the composite). Similar results

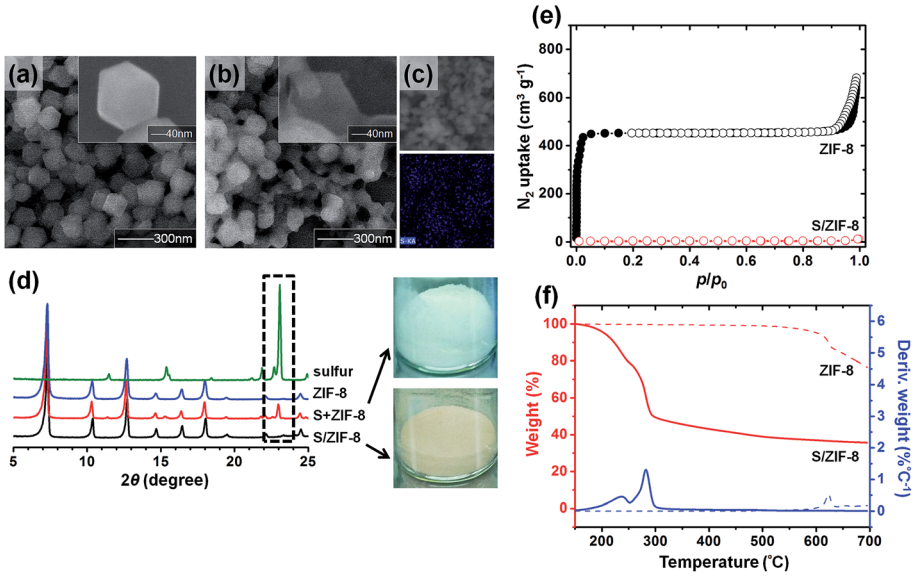

Fig. 3 Characterization of the sulfur infiltration of ZIF-8 nanocrystals: SEM images of (a) ZIF-8 nanocrystals and (b) S/ZIF-8. (c) EDS mapping of the sulfur distribution in S/ZIF-8. (d) PXRD patterns of sulfur and ZIF-8 after ground (S + ZIF-8) and after heated (S/ZIF-8). (e) N_2 adsorption isotherms of ZIF-8 and S/ZIF-8. (f) TGA of ZIF-8 and S/ZIF-8.

were obtained for the sulfur loading of MIL-53 (Fig. S1†), NH_2-MIL-53 (Fig. S2†), HKUST-1 (Fig. S3†), ZIF-8-M (Fig. S4†) and ZIF-8-L (Fig. S5†).

S/MOFs were first cycled between 1.8 and 2.8 V at various discharge/charge rates from 0.1 C to 1 C then back to 0.1 C (Fig. 4a). Contrary to the previously reported S/MIL-100,[29] where the highest capacity was achieved in the first discharge followed by an abrupt drop, all the S/MOFs in our study exhibit an activation process in the initial period. This phenomenon was previously found in systems where the accessibility of sulfur to the electrolyte is limited at the beginning;[50] owing to the smaller pore sizes of our MOFs compared to MIL-100, along with the

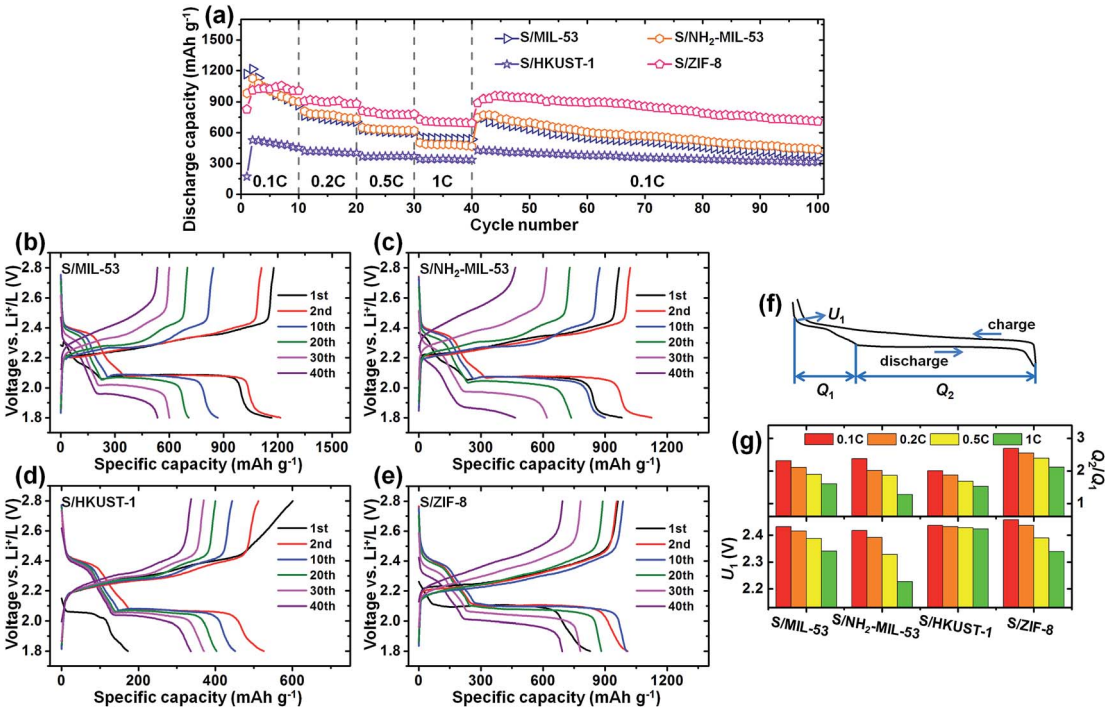

Fig. 4 Rate capabilities of S/MOFs: (a) discharge capacities. Voltage profiles of (b) S/MIL-53 (Al), (c) S/NH_2-MIL-53 (Al), (d) S/HKUST-1, and (e) S/ZIF-8. (f) Schematic of a typical voltage profile. U_1 is the onset potential of the upper plateau. Q_1 and Q_2 are the discharge capacities in stages 1 and 2, respectively. (g) The dependence of Q_2/Q_1 and U_1 on the current rate (data are collected from b–e).

higher sulfur loadings, it takes time for sulfur inside the pores to become fully electrochemically active. The maximum discharge capacities achieved after the activation process are 1215, 1125 and 1055 mA h g^{-1} at 0.1 C for S/MIL-53, S/NH_2-MIL-53 and S/ZIF-8, respectively. Such high utilizations of sulfur in these S/MOFs demonstrate that even sulfur stored in an electronically insulating microporous host can still be highly electrochemically active in an electrolyte with low viscosity and high polysulfide solubility.[48] However, the maximum discharge capacity for S/HKUST-1 is only as low as 526 mA h g^{-1} at 0.1 C. This can be ascribed to the extraordinarily large particle size of over 10 μm for HKUST-1 crystals (Fig. S3a†): according to $t \approx L^2/D$,[2,4] L for HKUST-1 is at least two times that of MIL-53, the second largest MOF in our study (in particle size, Fig. S1a†); thus t for HKUST-1 is at least four times that of MIL-53, extremely unfavorable for Li^+/e^- transport. Impressively, the small ZIF-8 nanocrystals of 100–200 nm yielded *via* the mechanochemical synthesis show excellent rate capabilities: even at a high discharge/charge rate of 1 C, S/ZIF-8 can still deliver a high reversible capacity of more than 710 mA h g^{-1}. More importantly, over 950 mA h g^{-1} can be recovered when the current rate was switched back to 0.1 C again, demonstrating the robustness of the MOF host in response to abrupt current changes. After 60 cycles at 0.1 C, the capacity still stands at 710 mA h g^{-1}, exceeding MIL-100 (ref. 29) in both electrode capacity and cycling stability.

All the S/MOFs undergo a two-plateau behavior of a typical sulfur cathode (Fig. 4b–e), which could be classified into two stages as follows (Fig. 4f):

$$S_8 + 4e^- \leftrightarrow 2S_4^{2-} \quad (1)$$

$$Q_1 = 1/4Q_0,\ Q_0 = 1675\ \text{mA h g}^{-1}$$

$$2S_4^{2-} + (12 - 2n)e^- + (16 - 2n)Li^+ \leftrightarrow nLi_2S_2 + (8 - 2n)Li_2S \quad (2)$$

$$Q_2 = (3/4 - n/8)Q_0,\ 0 \le n \le 4,\ 2 \le Q_2/Q_1 \le 3$$

Stage 1 corresponds to the formation of a liquid cathode through the reduction of element sulfur to soluble polysulfides, which amounts to 1/4 of the theoretical capacity. Stage 2 from the beginning of the lower plateau is the reduction of polysulfides to insoluble species (Li_2S_2 and Li_2S), accounting for 1/2 to 3/4 of the total capacity.[7,51] While the onset potential (U_1) of the upper plateau can reflect the interfacial kinetics, the capacity ratio of Q_2 to Q_1 (Q_2/Q_1) is a good indicator to evaluate the Li^+/e^- transport within the MOF host.[51] Fig. 4g shows the evolutions of U_1 and Q_2/Q_1 during the increase of current density. Among the four S/MOFs, S/ZIF-8 achieves the highest U_1 of 2.46 V and the highest Q_2/Q_1 of 2.7 at 0.1 C; Q_2/Q_1 still remains at a high ratio of 2.1 at 1 C. These results together highlight the merit of the uniform nanosized ZIF-8 hosts in terms of (i) promoting a more homogeneous mixing with the conductive matrix and (ii) facilitating Li^+/e^- transport across shorter dimensions. S/MIL-53, though exhibiting high U_1 of 2.43 V and considerable Q_2/Q_1 of 2.3 at 0.1 C, suffers from a fast drop in Q_2/Q_1 upon increase of the current rate; things are even worse in its counterpart, S/NH_2-MIL-53, accompanied by a rapid decline in U_1. Clearly, the 1D pathways in these two MOFs are rather disadvantageous for ion motion, like the case in bulk $LiFePO_4$.[52] In addition, the Lewis basic amino groups in NH_2-MIL-53, while in one hand are unfavorable for the generation and stabilization of the polysulfide phase, raising the energy barrier for charge transfer,[38] in another hand increase the hindrance of the MOF channels, dampening the ion diffusion. In contrast, the Lewis acidic open metal sites in HKUST-1,[44] while on interfacial kinetics, are beneficial for stabilizing the negatively charged redox centers, on internal Li^+/e^- transport, however, are unfavorable for anchoring the anions and retarding their exchange of Li^+/e^-. The former effect is suggested by the smallest decrease in U_1 among the four S/MOFs, while the latter is evident by the lowest Q_2/Q_1 of 2.0 even at 0.1 C.

To study how the sizes of MOF hosts affect the performance, microsized ZIF-8, ZIF-8-M (Fig. S4†) and ZIF-8-L (Fig. S5†), with an average size of 1 μm and 3 μm, respectively, are used as a prototype in comparison with their nanosized counterpart (150 nm on average). The three S/ZIF-8 composites were tested under a constant discharge/charge rate of 0.5 C for 100 cycles (Fig. 5a). In spite of the similar cycling stabilities (indeed downsized MOFs show a bit better retention), the major difference made by the particle size lies in reversible capacities: while 150 nm sized ZIF-8 can reach a discharge capacity of 733 mA h g^{-1}, ZIF-8 of 1 μm only delivers 556 mA h g^{-1}; this value further drops to 491 mA h g^{-1} when particle sizes increase to 3 μm (Fig. 5c black bars). The particle size does not give rise to a significant change in the shapes of voltage profiles (Fig. 5b); yet two trends are noteworthy. First, voltage hysteresis loops enlarge with downsized MOFs, indicating more and more insufficient electron transport from the given amount of conductive agent. This issue is common in nanoparticles since they have fewer points of contact with the conductive network to ensure electron transport than microsized materials.[4] Second, the ratio of Q_2/Q_1 increases with the downsizing of MOFs (Fig. 5c red bars). This feature, along with the higher reversible capacity, is the core benefit given by downsized MOFs: shorter diffusion lengths strongly facilitate the utilization of sulfur – more sulfur becomes electrochemically active with more Li^+/e^- per S atom. Overall, changing the particle sizes of MOF hosts mainly affect the internal Li^+/e^- transport, thus in turn the reversible capacity; cycling stability on the other hand receives less impact from the MOF particle size compared with the MOF structure itself – at least in the range of 100 nm to 3 μm. Therefore, if one is to preliminarily search for a potential candidate of MOF host, the particle size of the MOF can be taken into consideration as a secondary factor; only when one is to fully optimize the performance of a certain MOF should the particle size be carefully tailored.

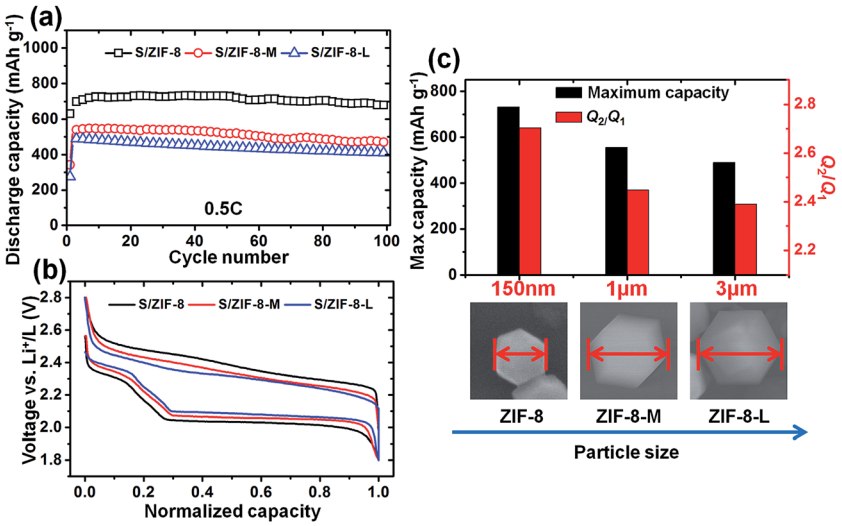

Fig. 5 Performances of S/ZIF-8 composites with different ZIF-8 particle sizes: (a) discharge capacities at 0.5 C. (b) Voltage profiles with normalized capacities. (c) The dependence of maximum discharge capacity and Q_2/Q_1 on the particle size (data are collected from a and b).

The S/MOFs were next tested under a constant discharge/charge rate of 0.5 C over 300 cycles to examine their long-term cyclabilities (Fig. 6a). The maximum discharge capacities achieved during the cycling process are 738, 431, 568 and 793 mA h g^{-1} for S/ZIF-8, S/HKUST-1, S/NH_2-MIL-53 and S/MIL-53, respectively. After the initial stages of activation, all S/MOFs show remarkable capacity retention over prolonged cycling. At the end of 300 cycles, their discharge capacities are 553, 286, 332 and 347 mA h g^{-1} for S/ZIF-8, S/HKUST-1, S/NH_2-MIL-53 and S/MIL-53, respectively, accounting for 75%, 66%, 58% and 44% of their maximum capacities.

The fading in the four S/MOF systems seems to be directly linked with the window sizes of the MOF pores (Fig. 6b). The diameters of the largest aperture (Fig. 6c) in ZIF-8, HKUST-1, NH_2-MIL-53 and MIL-53 are 3.4,[42] 6.9,[44] 7.5,[53] and 8.5 Å,[39] respectively, corresponding to the average decay rates of 0.08%, 0.11%, 0.14%, and 0.19% per cycle at 0.5 C and 0.43%, 0.45%, 0.72% and 0.82% per cycle at 0.1 C. MIL-100, which has a hexagonal window of 8.6 Å,[29] has a similar decay rate (~0.83% per cycle at 0.1 C, initial decay was excluded) with MIL-53, but decays faster than the other three MOFs. Specifically, the diameter of a S_8 ring is 6.9 Å;[13] this may suggest as a first approximation that the immobilizing effect given by an open framework with a window size larger than 6.9 Å would be substantially weakened (as displayed by MIL-53 and MIL-100 (ref. 29)). Note that the decay rates at 0.1 C are approximately five times those at 0.5 C for S/ZIF-8 and S/NH_2-MIL-53, which may imply that the leaching of polysulfides from the two MOF hosts is just proportional to the time for them to leach, and that the chemical environment inside the two MOFs has no additional gain in polysulfide confinement. Comparatively, this factor is 3.9 and 4.4 for S/HKUST-1 and S/MIL-53, respectively, indicating some extra immobilizing effect from the internal environment. During the review process, we noticed that a very recent work showed an excellent MOF host with a large window size of 13.8 Å having high cycling stability.[32] This can be taken as an example of a strong immobilizing effect posed by the internal environment (strong Lewis acidic centers) to compensate its relatively large apertures.

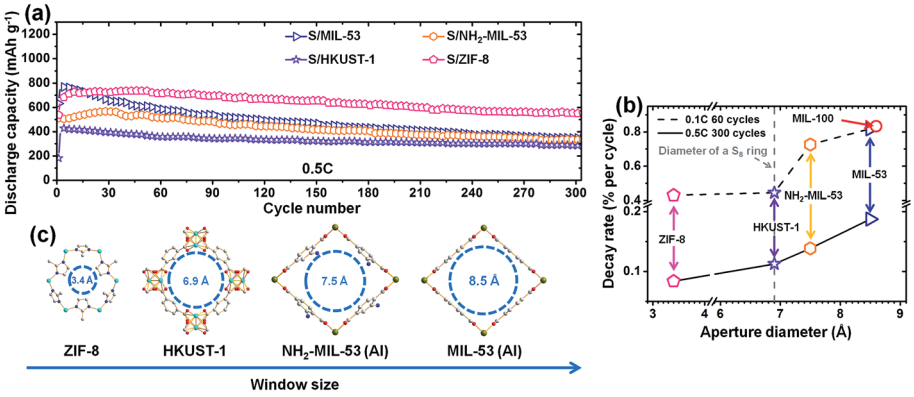

Fig. 6 Long-term cyclabilities of S/MOFs: (a) discharge capacities at 0.5 C. (b) Average decay rate as a function of the window size of the MOF host. The decay rate for MIL-100 was calculated based on Fig. 2 in ref. 29. (c) Schematic of the largest apertures of the four MOFs.

Fig. 7 illustrates the schematic model of the S/MOF system in the discharge process. Because the MOF host is electronically insulating, electrochemical reactions initiate on the surfaces of MOFs, more specifically, at the entrances of the pores, where the active mass can get access to Li^+/e^-. Sulfur in the outermost areas of the MOF particles is first reduced to long-chain polysulfides. Once generated, they can: (i) exchange Li^+/e^- with sulfur (or polysulfides) through the MOF channels (internal transport), (ii) be directly reduced to shorter chain species by the electrode (interfacial charge transfer), and (iii) escape from the MOF host (escape diffusion). While the escape diffusion (iii) is directly linked with capacity fading, the competition between internal transport (i) and interfacial charge transfer (ii) determines the amount of capacity that can be delivered before the total reaction is terminated by the complete blockage of the pores with the generation of Li_2S_2/Li_2S.[54,55]

To help evaluate the relative importance of these processes, electrochemical impedance spectroscopy (EIS) measurements were carried out at different discharge and charge states during the 2nd cycle at 0.1 C after the initial activation (Fig. 8). Only one semicircle in the high-frequency (HF) region reflecting the charge transfer process at the conductive matrix interface is observed among all S/MOFs at all states; the semicircle normally in the middle-frequency (MF) range attributed to the formation of an insulating film on the carbon matrix does not appear.[50,54] According to the fitting analysis of the Nyquist plots, the solution resistances (R_s) for all S/MOFs amount to a negligible contribution to the total resistance and do not show significant change during the whole process, indicating that the MOF hosts are effective in suppressing the escape diffusion (iii). The charge transfer resistances (R_{ct}), in contrast, vary a lot among different S/MOFs, from over a thousand Ohms in S/ZIF-8 to several tens of Ohms in S/HKUST-1. The combination of the fastest interfacial kinetics and the lowest specific capacity for S/HKUST-1 here again emphasizes the importance of small dimensions to reduce Li^+/e^- transport distances. Also the best performance of S/ZIF-8 associated with the highest R_{ct} indicates that the internal transport (i) is more likely to be the limiting factor in fully utilizing the active materials than the interfacial charge transfer (ii). Note that in all S/MOFs, R_{ct} reaches the minimum at the end of discharge, indicating that a considerable amount of soluble species still exist at the cutoff voltage of 1.8 V (remember that polysulfides facilitate charge transfer!) as we wanted and the blockage of the pores by the insoluble species is not severe. This can explain the systematic improvement in cycling reversibility among all S/MOFs just by setting the cutoff voltage for discharge at 1.8 V.

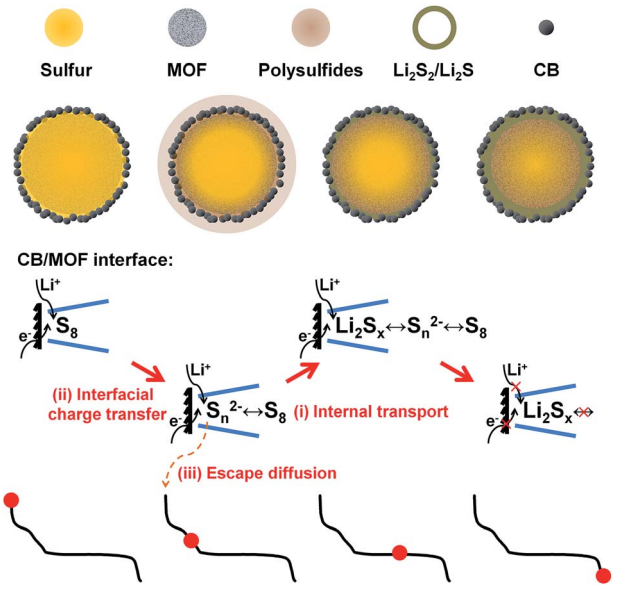

Fig. 7 Schematic model of the S/MOF system in the discharge process.

We have also tested the batteries between 1.6 and 2.8 V at various discharge/charge rates. Fig. 9 shows the results at 0.1 C. At first glance, the cycling behaviors are quite similar to those previously reported ones,[29–31] that is, a sharp decay occurs in the early period before the cycling becomes stable: 27%–57% in Fig. 8e, ~30% for MIL-100 (ref. 29), > 70% for HKUST-1 (ref. 30) and >50% for ZIF-8 (ref. 31). Sulfur loading may become the first concern (the sulfur loading effect is discussed in detail in the ESI, see Fig. S6†). Since the sulfur loadings in our study, both in the composite (50 wt%) and in the cathode (30 wt%), are higher than those in previous reports,[29–31] if the sulfur on the external surfaces of the MOF particles is the major contributor to the initial decay, a systematically larger decay would be observed in our S/MOFs, but this is not the case. A second concern may come from the concentration of the LiTFSI salt. We used a lower molarity electrolyte (0.6 M) compared with those reports (1 M).[29–31] Since a low molarity electrolyte tends to dissolve more polysulfides and leads to more severe capacity fadings,[10,36] clearly, it cannot explain the absence of intense fading in our study when the cutoff voltage for discharge was set at 1.8 V. Careful comparison of the voltage profiles in Fig. 4 and 9 reveals that a significant amount of capacity is released within the voltage range between 1.6 V and 1.8 V in the first discharge, which substantially shrinks in the second cycle. This irreversible capacity cannot be attributed to the reduction of $LiNO_3$, because (i) irreversible capacities given by $LiNO_3$ are often present as two long voltage plateaus at 1.6 V and 1.3 V,[56] and (ii) the same concentration of $LiNO_3$ was also used as an additive in previous reports and no irreversible capacities were present even after the batteries were discharged to 1.0 V.[30,31]

We interpret this irreversible capacity as follows, and a schematic model is illustrated in Fig. 9f. Because of the high sulfur contents in our S/MOFs (little room for accommodation of the volume change), the entrances of the MOF pores are easier to be blocked by the formation of insoluble species in the late period of discharge, since the volume expansion caused by lithiation initiates from the outermost areas of the particles. When the surfaces of a MOF particle are fully covered by the insoluble species, its core areas still remain highly lithium deficient. Deeper discharge needs to overcome the barriers of this surface coating, for the transport of both electrons and Li ions, rendering an extra polarization. After discharged to 1.6 V, the whole MOF pores are full of an insoluble Li_2S_2/Li_2S mixture; because of its lower density, much of it spreads out of the pores

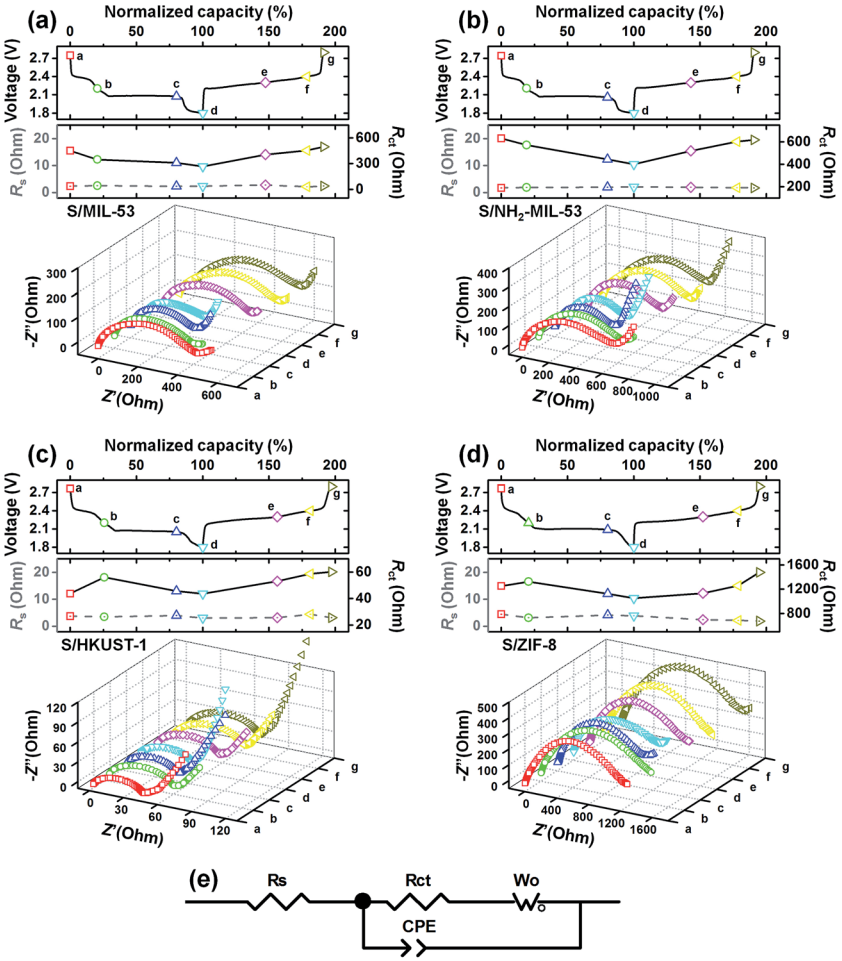

Fig. 8 EIS measurements at different discharge and charge states during the 2nd cycle at 0.1 C: (a) S/MIL-53 (Al), (b) S/NH_2-MIL-53 (Al), (c) S/HKUST-1, and (d) S/ZIF-8. In each figure of (a–d), the labels of a, b, …, g in the Nyquist plots (bottom) refer to the discharge or charge states in the voltage profile (top). At each state, solution resistances (R_s) and charge transfer resistances (R_{ct}) are obtained (middle) by fitting to (e) the equivalent circuit model in analysing the Nyquist plots.

and accumulates on the surfaces, leading to a volume expansion of the whole particle. This expansion causes (i) a great damage to the electrical contact with the conductive matrix, and (ii) much of the active mass to escape from the MOF host; both are responsible for the large initial decay.[24,50] Therefore a deep discharge definitely weakens the advantage of a MOF host.

Another disadvantage associated with the deep discharge is that a large potential barrier is apparent at the beginning of the first charge (Fig. 9a–d), which does not occur if discharged only to 1.8 V (Fig. 4b–e). With the lack of the polysulfide phase, the oxidation of Li_2S_2/Li_2S is extremely sluggish, which has been fully discussed in previous literature.[38] This emphasizes the important role of dissolved polysulfides in exchanging Li^+/e^- and accelerating the electrochemical kinetics. Here to set the cutoff voltage for discharge to 1.8 V provides a mild activation procedure in a way that polysulfides are always available in the MOF channels to facilitate the kinetics both in charge and discharge.

The addition of $LiNO_3$ can be a considerable factor in the S/MOF system. According to previous reports,[12,32,57] $LiNO_3$ as an electrolyte additive mainly helps to enhance the Coulombic efficiency, whereas no improvement was shown on cycling stability solely based on the addition of $LiNO_3$.[58] Since the introduction of MOFs brings further complexity to the Li–S system, to fully understand the effect of each component and the underlying mechanism in such a system remains challenging. We did not rule out the synergetic effect of $LiNO_3$ when MOF was used as the host for sulfur. Hence, we carefully evaluated the dependence of electrochemical performance of S/ZIF-8 on the addition of $LiNO_3$ (Fig. S7†). The shapes of voltage profiles are similar (Fig. S7a and S7b†), indicating no significant influence by $LiNO_3$ on the electrochemical reactions of active sulfur in the presence of MOF. Cycling stability does not show significant change in the absence of $LiNO_3$ (Fig. S7c†); Coulombic efficiency, however, is the main difference, as the average level decreases from *ca.* 101% (with $LiNO_3$) to *ca.* 95% (without $LiNO_3$). These results are in line with previous reports;[12,32,57] therefore it is reasonable to conclude that the main contributor to the stable cycling behaviour in the S/MOF system is the confinement effect of MOF. However, there is no

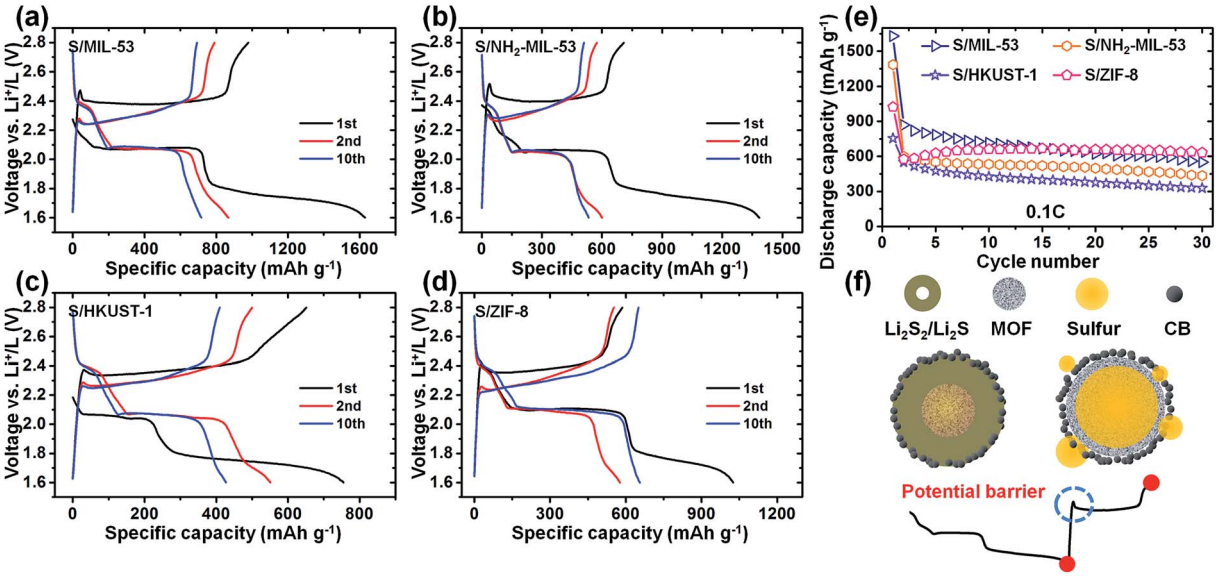

Fig. 9 Performances of S/MOFs between 1.6 and 2.8 V at 0.1 C: voltage profiles for (a) S/MIL-53 (Al), (b) S/NH_2-MIL-53 (Al), (c) S/HKUST-1, and (d) S/ZIF-8. (e) Discharge capacities. (f) Schematic model of the S/MOF system under deep discharge.

doubt that further research and systematic study are needed to fully understand the fundamental mechanism.

Conclusions

MOFs are a promising platform to search for an effective host to store sulfur and retain the soluble polysulfides through rational design and systematic adjustment. In conjunction with an electrolyte highly dissolving polysulfides and an appropriate voltage range of 1.8–2.8 V, sulfur stored in a MOF host can take advantage of both intercalation (fast and stable) and conversion (high energy density) cathodes, for the mobile dielectron redox centers are well-trapped in the well-defined host for the reversible and efficient insertion/extraction of Li^+/e^-. We have demonstrated ZIF-8 nanocrystals, made from a simple mechanochemical synthetic protocol, as an effective host. Prominent rate capabilities with exceptional capacity retention are achieved by virtue of a small window size of 3.4 Å plus a small and uniform particle size of 100–200 nm. By comparing with another three distinct MOFs, MIL-53 (Al), NH_2-MIL-53 (Al), and HKUST-1, along with two microsized ZIF-8 with different average particle sizes, useful guides for the rational design of a MOF host are elucidated. The performance of the as-designed cathode is governed by the internal transport of Li^+/e^- and the escape diffusion of polysulfides: the former determines the utilization of sulfur, and the latter dominates capacity retention. Decreasing the particle size of the MOF host is appreciable to achieve a high capacity. Small apertures, associated with functionalities in the open framework that have affinity with the polysulfide anions, can help achieve a stable cycling. Further directions for developing the S/MOF system are straightforward: (i) applying a more effective and flexible conductive matrix, such as carbon nanotubes[14] and graphene,[28] to enhance the overall conductivity, (ii) preparing smaller nanoparticles[45] of MOFs to fully optimize sulfur utilization and rate capabilities, and (iii) using MOFs with giant cages (and small windows)[59] to increase sulfur loading.[32] Specifically, in the case of HKUST-1, as expected,[32] the open metal centers serve as the Lewis acidic sites with high affinity to the negatively charged polysulfide anions and largely enhance capacity retention. In order to fully understand the effect of the metal centers, it is necessary to compare them in series of MOFs with identical underlying topology. By doing so, one can rule out the impact of pores and organic links. We believe that these guides are general and applicable for the rational design of new hosts for sulfur in other porous materials families[60] to produce more effective and stable Li–S batteries.

Acknowledgements

This work is supported by the Ministry of Science and Technology of China (no. 2010CB631301) and the National Natural Science Foundation of China (no. U1201241, 11375020 and 21321001).

Notes and references

1 M. Armand and J. M. Tarascon, *Nature*, 2008, **451**, 652.
2 A. S. Arico, P. Bruce, B. Scrosati, J. M. Tarascon and W. Van Schalkwijk, *Nat. Mater.*, 2005, **4**, 366.
3 J. B. Goodenough and K.-S. Park, *J. Am. Chem. Soc.*, 2013, **135**, 1167.
4 P. G. Bruce, B. Scrosati and J.-M. Tarascon, *Angew. Chem., Int. Ed.*, 2008, **47**, 2930.
5 X. Ji and L. F. Nazar, *J. Mater. Chem.*, 2010, **20**, 9821.
6 P. G. Bruce, S. A. Freunberger, L. J. Hardwick and J.-M. Tarascon, *Nat. Mater.*, 2012, **11**, 19.
7 Y. Yang, G. Zheng and Y. Cui, *Chem. Soc. Rev.*, 2013, **42**, 3018.

8 B. L. Ellis, K. T. Lee and L. F. Nazar, *Chem. Mater.*, 2010, **22**, 691.
9 X. Ji, K. T. Lee and L. F. Nazar, *Nat. Mater.*, 2009, **8**, 500.
10 J. T. Lee, Y. Zhao, S. Thieme, H. Kim, M. Oschatz, L. Borchardt, A. Magasinski, W.-I. Cho, S. Kaskel and G. Yushin, *Adv. Mater.*, 2013, **25**, 4573.
11 R. Elazari, G. Salitra, A. Garsuch, A. Panchenko and D. Aurbach, *Adv. Mater.*, 2011, **23**, 5641.
12 G. Zheng, Y. Yang, J. J. Cha, S. S. Hong and Y. Cui, *Nano Lett.*, 2011, **11**, 4462.
13 S. Xin, L. Gu, N.-H. Zhao, Y.-X. Yin, L.-J. Zhou, Y.-G. Guo and L.-J. Wan, *J. Am. Chem. Soc.*, 2012, **134**, 18510.
14 Y. Fu, Y.-S. Su and A. Manthiram, *Angew. Chem., Int. Ed.*, 2013, **52**, 6930.
15 B. Zhang, X. Qin, G. R. Li and X. P. Gao, *Energy Environ. Sci.*, 2010, **3**, 1531.
16 J. Schuster, G. He, B. Mandlmeier, T. Yim, K. T. Lee, T. Bein and L. F. Nazar, *Angew. Chem., Int. Ed.*, 2012, **51**, 3591.
17 L. Ji, M. Rao, H. Zheng, L. Zhang, Y. Li, W. Duan, J. Guo, E. J. Cairns and Y. Zhang, *J. Am. Chem. Soc.*, 2011, **133**, 18522.
18 H. Wang, Y. Yang, Y. Liang, J. T. Robinson, Y. Li, A. Jackson, Y. Cui and H. Dai, *Nano Lett.*, 2011, **11**, 2644.
19 S. Evers and L. F. Nazar, *Chem. Commun.*, 2012, **48**, 1233.
20 J. L. Wang, J. Yang, J. Y. Xie and N. X. Xu, *Adv. Mater.*, 2002, **14**, 963.
21 L. Xiao, Y. Cao, J. Xiao, B. Schwenzer, M. H. Engelhard, L. V. Saraf, Z. Nie, G. J. Exarhos and J. Liu, *Adv. Mater.*, 2012, **24**, 1176.
22 G. Zheng, Q. Zhang, J. J. Cha, Y. Yang, W. Li, Z. W. Seh and Y. Cui, *Nano Lett.*, 2013, **13**, 1265.
23 K. T. Lee, R. Black, T. Yim, X. Ji and L. F. Nazar, *Adv. Energy Mater.*, 2012, **2**, 1490.
24 Z. W. Seh, W. Li, J. J. Cha, G. Zheng, Y. Yang, M. T. McDowell, P.-C. Hsu and Y. Cui, *Nat. Commun.*, 2013, **4**, 1331.
25 X. Ji, S. Evers, R. Black and L. F. Nazar, *Nat. Commun.*, 2011, **2**, 325.
26 S. Evers, T. Yim and L. F. Nazar, *J. Phys. Chem. C*, 2012, **116**, 19653.
27 Y.-S. Su and A. Manthiram, *Nat. Commun.*, 2012, **3**, 1166.
28 G. Zhou, S. Pei, L. Li, D.-W. Wang, S. Wang, K. Huang, L.-C. Yin, F. Li and H.-M. Cheng, *Adv. Mater.*, 2014, **26**, 625.
29 R. Demir-Cakan, M. Morcrette, F. Nouar, C. Davoisne, T. Devic, D. Gonbeau, R. Dominko, C. Serre, G. Férey and J.-M. Tarascon, *J. Am. Chem. Soc.*, 2011, **133**, 16154.
30 Z. Wang, X. Li, Y. Cui, Y. Yang, H. Pan, Z. Wang, C. Wu, B. Chen and G. Qian, *Cryst. Growth Des.*, 2013, **13**, 5116.
31 Z. Wang, Z. Dou, Y. Cui, Y. Yang, Z. Wang and G. Qian, *Microporous Mesoporous Mater.*, 2014, **185**, 92.
32 J. Zheng, J. Tian, D. Wu, M. Gu, W. Xu, C. Wang, F. Gao, M. H. Engelhard, J.-G. Zhang, J. Liu and J. Xiao, *Nano Lett.*, 2014, **14**, 2345.
33 S. Kitagawa, R. Kitaura and S. Noro, *Angew. Chem., Int. Ed.*, 2004, **43**, 2334.
34 G. Ferey, *Chem. Soc. Rev.*, 2008, **37**, 191.
35 H. Furukawa, K. E. Cordova, M. O'Keeffe and O. M. Yaghi, *Science*, 2013, **341**, 974.
36 L. Suo, Y.-S. Hu, H. Li, M. Armand and L. Chen, *Nat. Commun.*, 2013, **4**, 1481.
37 Y. Yang, G. Y. Zheng and Y. Cui, *Energy Environ. Sci.*, 2013, **6**, 1552.
38 Y. Yang, G. Zheng, S. Misra, J. Nelson, M. F. Toney and Y. Cui, *J. Am. Chem. Soc.*, 2012, **134**, 15387.
39 T. Loiseau, C. Serre, C. Huguenard, G. Fink, F. Taulelle, M. Henry, T. Bataille and G. Ferey, *Chem.–Eur. J.*, 2004, **10**, 1373.
40 T. Ahnfeldt, D. Gunzelmann, T. Loiseau, D. Hirsemann, J. Senker, G. Ferey and N. Stock, *Inorg. Chem.*, 2009, **48**, 3057.
41 S. S. Y. Chui, S. M. F. Lo, J. P. H. Charmant, A. G. Orpen and I. D. Williams, *Science*, 1999, **283**, 1148.
42 K. S. Park, Z. Ni, A. P. Cote, J. Y. Choi, R. Huang, F. J. Uribe-Romo, H. K. Chae, M. O'Keeffe and O. M. Yaghi, *Proc. Natl. Acad. Sci. U. S. A.*, 2006, **103**, 10186.
43 M. Pera-Titus, T. Lescouet, S. Aguado and D. Farrusseng, *J. Phys. Chem. C*, 2012, **116**, 9507.
44 J. L. C. Rowsell and O. M. Yaghi, *J. Am. Chem. Soc.*, 2006, **128**, 1304.
45 J. Cravillon, R. Nayuk, S. Springer, A. Feldhoff, K. Huber and M. Wiebcke, *Chem. Mater.*, 2011, **23**, 2130.
46 R. Li, X. Ren, J. Zhao, X. Feng, X. Jiang, X. Fan, Z. Lin, X. Li, C. Hu and B. Wang, *J. Mater. Chem. A*, 2014, **2**, 2168.
47 D. Aurbach, E. Pollak, R. Elazari, G. Salitra, C. S. Kelley and J. Affinito, *J. Electrochem. Soc.*, 2009, **156**, A694.
48 S. S. Zhang, *J. Power Sources*, 2013, **231**, 153.
49 R. Elazari, G. Salitra, Y. Talyosef, J. Grinblat, C. Scordilis-Kelley, A. Xiao, J. Affinito and D. Aurbach, *J. Electrochem. Soc.*, 2010, **157**, A1131.
50 W. Li, G. Zheng, Y. Yang, Z. W. Seh, N. Liu and Y. Cui, *Proc. Natl. Acad. Sci. U. S. A.*, 2013, **110**, 7148.
51 M.-S. Park, J.-S. Yu, K. J. Kim, G. Jeong, J.-H. Kim, Y.-N. Jo, U. Hwang, S. Kang, T. Woo and Y.-J. Kim, *Phys. Chem. Chem. Phys.*, 2012, **14**, 6796.
52 A. K. Padhi, K. S. Nanjundaswamy and J. B. Goodenough, *J. Electrochem. Soc.*, 1997, **144**, 1188.
53 S. Couck, T. Remy, G. V. Baron, J. Gascon, F. Kapteijn and J. F. M. Denayer, *Phys. Chem. Chem. Phys.*, 2010, **12**, 9413.
54 L. Yuan, X. Qiu, L. Chen and W. Zhu, *J. Power Sources*, 2009, **189**, 127.
55 C. Barchasz, J.-C. Lepretre, F. Alloin and S. Patoux, *J. Power Sources*, 2012, **199**, 322.
56 S. S. Zhang, *Electrochim. Acta*, 2012, **70**, 344.
57 X. Liang, Z. Wen, Y. Liu, M. Wu, J. Jin, H. Zhang and X. Wu, *J. Power Sources*, 2011, **196**, 9839.
58 L. Suo, Y.-S. Hu, H. Li, M. Armand and L. Chen, *Nat. Commun.*, 2013, **4**, 1481.
59 B. Wang, A. P. Cote, H. Furukawa, M. O/'Keeffe and O. M. Yaghi, *Nature*, 2008, **453**, 207.
60 B. K. Guo, T. Ben, Z. H. Bi, G. M. Veith, X. G. Sun, S. L. Qiu and S. Dai, *Chem. Commun.*, 2013, **49**, 4905.

